

# Study on crack propagation simulation of surface crack in welded joint structure

Satoyuki Tanaka<sup>a</sup>, Takahiro Kawahara<sup>a</sup>, Hiroshi Okada<sup>b</sup>

<sup>a</sup>*Graduate School of Engineering, Hiroshima University,  
4-1, Kagamiyama 1-chome, Higashi-Hiroshima, 739-8527, Japan,  
e-mail: satoyuki@hiroshima-u.ac.jp, m146691@hiroshima-u.ac.jp*

<sup>b</sup>*Department of Mechanical Engineering, Faculty of Science and Technology,  
Tokyo University of Science, 2641 Yamazaki, Noda, 278-8510, Japan,  
e-mail: hokada@rs.noda.tus.ac.jp*

---

## Abstract

Recently developed computational techniques are applied to the simulation of the crack propagation of a surface crack in a welded joint. The results are compared with those obtained by the conventional techniques. Three approaches are adopted: three-dimensional finite element analysis using quadratic tetrahedral finite elements; the two-dimensional extended finite element method using the  $Mk$  factor; and the use of three-dimensional  $Mk$  factor formulae. In the numerical examples, stress intensity factors,  $Mk$  factors, crack paths and fatigue cycles are evaluated for a surface crack in a T-shaped welded joint. The accuracy and effectiveness of the approaches are discussed.

*Keywords:* Finite Element Method, Extended Finite Element Method, Welded Joints, Surface Crack, Crack Propagation Analysis

---

## 1. Introduction

Welded joints are often adopted in ships and ocean structures. Evaluation of fatigue strength of the welded joints is important in assessing the structural integrity of welded structures. The detailed description for mechanics of materials, fatigue and fracture are given in [1-5]. Methods of evaluation include fracture mechanics analysis and crack propagation simulation. So far, several analytical/numerical approaches have been proposed and new computational techniques have been developed. Additionally, simulations for complex shape geometry are easily handled by advances in computer power.

Fracture mechanics analysis and crack propagation simulations are conducted to evaluate the fatigue crack growth life of welded joints. To carry out such simulations, the stress intensity factor (SIF) of cracks embedded at the weld toe should be evaluated accurately. However, there are difficulties in obtaining the SIF of cracks because the welded joints have complex geometry, and they have a crack front singularity and high stress concentration near the weld. Weld toe magnification factor ( $Mk$  factor) can be used to evaluate the SIF of a surface crack located at the weld toe. The  $Mk$  factor was originally proposed by Maddox [6] to quantify the change in stress intensity due to the presence of welded attachments. The SIF of a surface crack located at the weld toe can be predicted from formulae for the  $Mk$  factor and reference SIF solutions of a surface crack on a rectangular plate; *i.e.*, the so-called Raju-Newman solution [7]. In addition, simplified prediction of the crack propagation can be carried out by adopting the Paris law [8]. The  $Mk$  factor is evaluated using two-dimensional (2D) or three-dimensional (3D) welded joint models. In this paper, the  $Mk$  factors in 2D and 3D cases are denoted  $Mk_{(2D)}$  and  $Mk_{(3D)}$ , respectively. Simplified formulae for the  $Mk$  factor have been proposed for several types of welded joints and have been included in standard specifications: *e.g.*, BS7910 [9] and WES2805 [10]. The use of the  $Mk$  factor is a simple and effective approach, and the  $Mk$  factor is used by service engineers in evaluating the structural integrity of welded structures.

In recent years, new computational techniques have been proposed to reduce the modeling tasks in crack analyses. Finite Element Analysis (FEA) is widely used in the fracture mechanics problems and the applications for

ships and ocean structures were carried out [11-16]. FEA using triangular or tetrahedral finite elements (FEs) is one such technique. The FE modeling of complicated geometry including cracks is made possible by software that automatically generates meshes. Techniques to compute the SIF have been proposed and employed in the simulation of crack propagation using triangular or tetrahedral elements [17-20]. Meshfree approaches, such as the element-free Galerkin method [21,22], eXtended finite element method (X-FEM) [23,24] and free mesh method [25,26] can reduce the modeling tasks for structures with complex shape. As one such approach, the X-FEM is suitable for solving crack problems and analyzing crack propagation; the new basis functions are introduced to the original displacement function of the finite element method (FEM) to represent the displacement discontinuity of the crack surface and the near crack tip asymptotic solutions. The crack propagation is effectively analyzed because relocations of the enrichment functions are performed without remeshing procedures. As another approach, the boundary element method [27-29] reduces the modeling tasks since only the surface meshing of cracked bodies is needed in the discretization.

In this study, propagation of a surface crack in a T-shaped welded joint is simulated using the new approaches of computational fracture mechanics. Although actual fatigue failure in welded joints starts multiple surface cracks and forms a very shallow surface crack along the stress concentration region, single semi-elliptical crack is assumed to validate the fracture mechanics analysis and crack propagation simulation. The results are compared with those obtained with conventional techniques. Three approaches are employed: (i) 3D FEA using quadratic tetrahedral FEs, (ii) the 2D X-FEM using the  $Mk_{(2D)}$ , and (iii) the use of  $Mk_{(3D)}$  formulae. In (i) 3D FEA using quadratic tetrahedral FEs, automatic mesh generation software [30] is adopted to model surface cracks in welded joints. The surface crack is defined by the 3D model directly and the FE model is automatically generated using the tetrahedral FEs. The virtual crack closure-integral method (VCCM) [31] is adopted to evaluate the SIFs. The remeshing is incrementally performed as the crack extends. For the (ii) 2D X-FEM using the  $Mk_{(2D)}$ , a method proposed by the authors [32] is adopted. The method is based on the wavelet FEM [33-35] and the X-FEM. The discretization is based on fixed grids (the so-called voxel approach) [36], and the approach is suitable for modeling complex shape geometries such as welded joints. Hereafter, the method is

referred to as the WX-FEM. Although the analysis is 2D, simplified propagation of a surface crack in a welded joint can be simulated using the  $Mk_{(2D)}$  and Raju-Newman solution. Furthermore, 3D crack propagation simulations are carried out using the  $Mk_{(3D)}$  formulae and Raju-Newman solution in the (iii)  $Mk_{(3D)}$  formulae approach. The Paris law is adopted for the crack growth law. The SIFs,  $Mk$  factors, crack paths and fatigue cycles obtained with the three approaches are compared, and the accuracy and effectiveness of the proposed approaches are discussed.

The paper is organized as follows. Section 2 presents crack propagation simulation using the  $Mk_{(3D)}$  formulae. Crack modeling and simulation of crack propagation using the tetrahedral FEs are described in section 3. Section 4 presents the simulation of crack propagation using the WX-FEM and  $Mk_{(2D)}$ . In section 5, propagation of surface cracks in T-shaped welded joints is simulated as numerical examples. Finally, conclusions are drawn in section 6.

## 2. Simulation of crack propagation using the $Mk$ factor

### 2.1. $Mk$ factor

A T-shaped welded joint structure including a surface crack is shown in Fig. 1 (a). The  $Mk$  factor is used to evaluate the mode-I SIF  $K$  of a surface crack at the weld toe. The  $Mk$  factor is defined as the ratio of the  $K$  value with and without the welded attachment:

$$Mk = \frac{K_{(in\ plate\ with\ attachment)}}{K_{(in\ same\ plate\ but\ with\ no\ attachment)}}. \quad (1)$$

Researchers [6,37-39] have evaluated the  $Mk$  factor using a 2D edge crack model ( $Mk_{(2D)}$ ) because it has been difficult to model a 3D welded joint model including a surface crack. However, it has been found that the estimation of the SIF using  $Mk_{(2D)}$  is overly conservative, and it was proposed to evaluate the  $Mk$  factor using a 3D model ( $Mk_{(3D)}$ ) and 3D FEA [40-42]. Bowness and Lee [43-45] proposed highly accurate formulae for  $Mk_{(3D)}$  in wide ranges of the aspect ratio of the surface crack, welded attachment thickness, main plate thickness and weld angle, for T-butt welded joints through a parametric study of 3D FEAs. In addition, simplified formulae of the  $Mk$

factor for several types of welded joints have been included in standard specifications [9,10], and the formulae can be adopted to evaluate behaviors of crack growth in welded joints using the Paris law.

## 2.2. Simulation of crack propagation using the $Mk_{(3D)}$

The mode-I SIF of a surface crack at the weld toe can be predicted employing the  $Mk$  factor formulae and Raju-Newman solution. In addition, simplified predictions of the crack propagation can be made to adopt the Paris law. The surface crack is assumed to initiate at the weld toe, and it grows under cyclic loadings. A flowchart of the crack propagation analysis using  $Mk_{(3D)}$  formulae is shown in Fig. 1 (b). The cross-section of a semi-elliptical surface crack and the local coordinates are shown in 1 (c). Global and local coordinates are denoted  $x_1, x_2, x_3$  and  $x'_1, x'_2, x'_3$ , respectively.  $\phi$  is an eccentric angle of the semiellipse. The depth of the surface crack is denoted  $a$  and the width is denoted  $2c$ . The crack growth from cycle  $N_k$  to cycle  $N_{k+1}$  is schematically presented as shown in Fig. 1 (d).  $\Delta a_k$  and  $\Delta c_k$  are crack growth increments at the deepest point and the crack ends in the  $k$ -th step of the calculation, respectively. Adopting  $Mk_{(3D)}$  formulae, propagation of a semi-elliptical surface crack at the weld toe is simulated according to the following procedures.

- (i) Employing the  $Mk_{(3D)}$  formulae and Raju-Newman solution,  $K$  of a surface crack in a welded joint is estimated at the deepest point  $K_a$  and at the crack ends  $K_c$ .
- (ii)  $\Delta K_a$  and  $\Delta K_c$  are evaluated using  $K_a$  and  $K_c$  obtained in procedure (i). The crack growth increments  $\Delta a_k$  and  $\Delta c_k$  in the  $k$ -th step are evaluated by substituting  $\Delta K_a$  and  $\Delta K_c$  into the Paris law.
- (iii)  $\Delta a_k$  and  $\Delta c_k$  are added to  $a_k$  and  $c_k$ , respectively. The geometry is updated for the computation of the  $k + 1$ -th crack propagation step as shown in Fig. 1 (d).

Procedures (i)-(iii) are repeated until the crack grows to the prescribed size. Because  $K$  is only evaluated at the deepest point and the crack ends, the developed surface crack maintains a semi-elliptical shape. In chapter 4, crack propagation simulations of a surface crack using  $Mk_{(2D)}$  are presented.

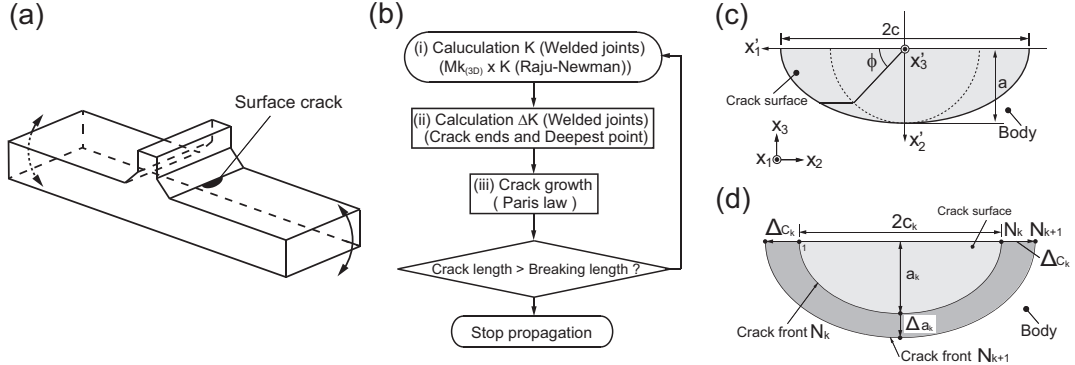


Figure 1: Procedures for simulating the propagation of a semi-elliptical surface crack using  $Mk_{(3D)}$ .

### 3. Simulation of crack propagation using tetrahedral FEs

VCCM (Virtual Crack Closure-Integral Method) employed to compute the SIFs is briefly described. In VCCM computations, only the nodal opening displacements and nodal forces at the crack front are needed to evaluate the SIFs. The mode splitting is relatively easy in the mixed-mode problem compared with the case in other SIF calculation techniques; *e.g.*, the  $J$ -integral [46] and virtual crack extension methods [47]. Okada *et al.* [31] proposed applying the VCCM calculation technique to 3D cracks using quadratic tetrahedral FEs.

Automatic mesh generation software is adopted to generate the FE welded joint model including surface cracks. The user interface of the FE pre-processing software (pre-software) [30] is shown in Fig. 2 (a). A surface crack can be directly defined in the 3D model and the FE modeling using quadratic tetrahedrons can be performed simply by one-click operation. The software is connected with MSC.NASTRAN [50] in a Windows operating system and the remeshing is executed incrementally in a batch process. Flowchart of the crack propagation simulation is presented in Fig. 2 (b). The simulation has the following procedures.

- (i) A 3D-CAD welded joint model is arranged and imported the CAD model into the pre-software.

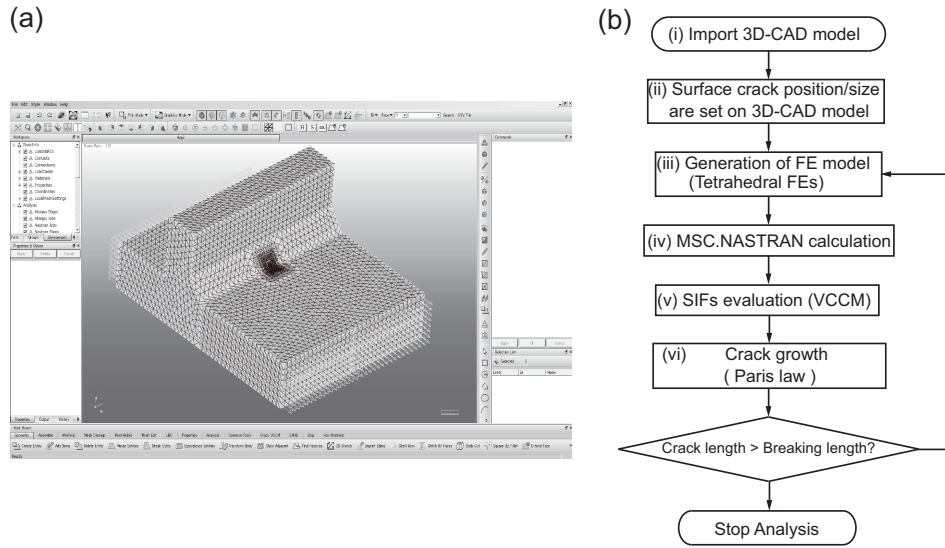


Figure 2: User interface and flowchart of a 3D crack propagation simulation system.

- (ii) The initial crack size is defined and the location of the surface crack is set in the model.
- (iii) Local settings of the mesh parameter are defined in the model. A mesh is automatically generated using quadratic tetrahedral FEs.
- (iv) The boundary and loading conditions are set for the FE model. Linear static analysis is performed using MSC.NASTRAN.
- (v) SIFs are evaluated using the VCCM technique in the post-processing software.
- (vi) Crack growth rates are evaluated using the SIFs. Because the  $K_I$ -dominant problem is only treated in this study,  $K_I$  is used to evaluate the crack growth rate and the surface crack always extends in the same plane. The crack geometry is updated.

Procedures (iii)-(vi) are repeated until the surface crack grows to the prescribed size. The crack surface in the FE model is shown in Fig. 3 (a). A schematic illustration of the crack propagation is shown in Fig. 3 (b). The surface crack extends from cycle  $N_k$  to cycle  $N_{k+1}$ . The nodes along the crack

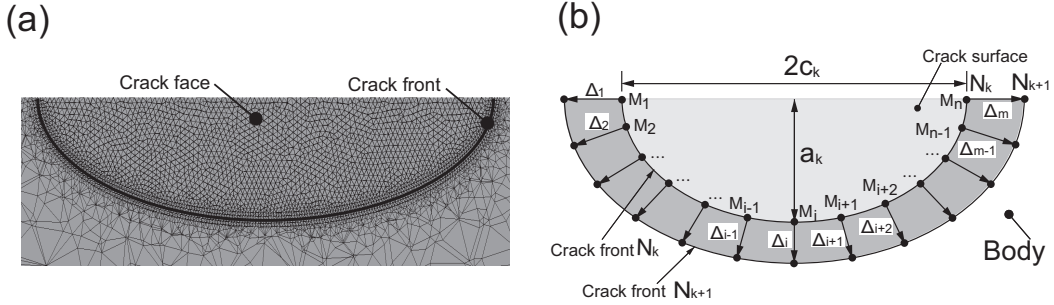


Figure 3: Cross-section of a surface crack in the FE model and schematic illustration of the crack propagation.

front are denoted  $M_i$  ( $i = 1, \dots, n$ ), and the crack growth increments are denoted  $\Delta_i$ , respectively. In the proposed approach, the crack growth rate and the crack growth direction are evaluated for all nodes along the crack front. Although it is known that a plane stress condition is assumed near the crack ends, a plane strain condition is assumed at all nodes of the crack front.

#### 4. Crack propagation simulation using 2D WX-FEM and $Mk_{(2D)}$

##### 4.1. Analysis of 2D crack problems using WX-FEM

The wavelet FEM [33,34] is a numerical technique used to solve partial differential equations. Wavelet functions are used as interpolation functions in the FEM framework. Spatial resolution of the analysis model is easy to control based on the multiresolution analysis in the wavelet theory [51,52]. A schematic illustration of the wavelet FEM is presented in Fig. 4. Linear B-spline scaling/wavelet functions are adopted as the basis functions. The lowest resolution is assumed level- $j$ . The level- $j$  scaling functions are periodically located to represent the low-resolution solution. In addition, the level- $j$  wavelet functions are adopted to represent the high-resolution solution. The wavelet functions can be superposed locally where a high-resolution approximation is needed such as stress concentration. In the fracture mechanics analysis, wavelet functions located in the radius  $r_e$  is employed. Equally spaced structured cells (level- $j$  cell) and sub-cells are adopted to accurately integrate the stiffness matrix including the wavelet functions. In the similar

manner, higher resolution wavelet functions (level- $j + 1, j + 2, \dots$ ) can be superposed subsequently to increase the spatial resolution.

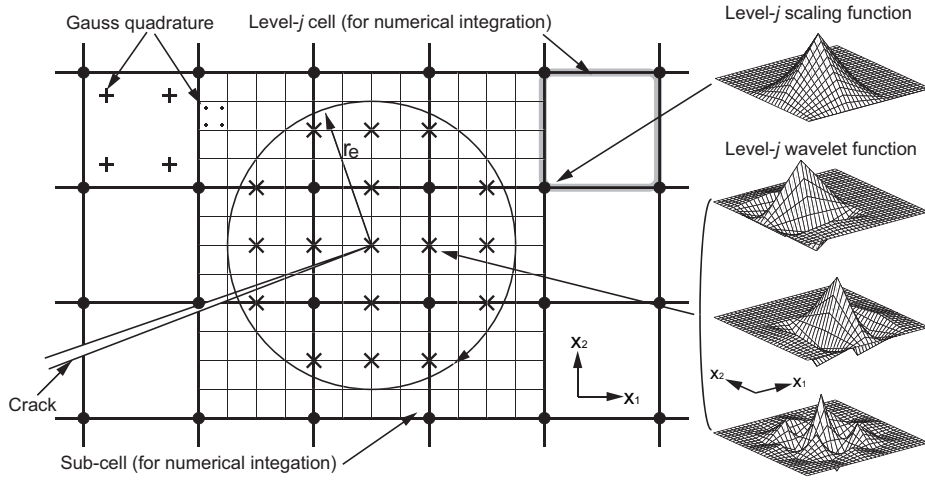


Figure 4: Wavelet FEM for crack problems.

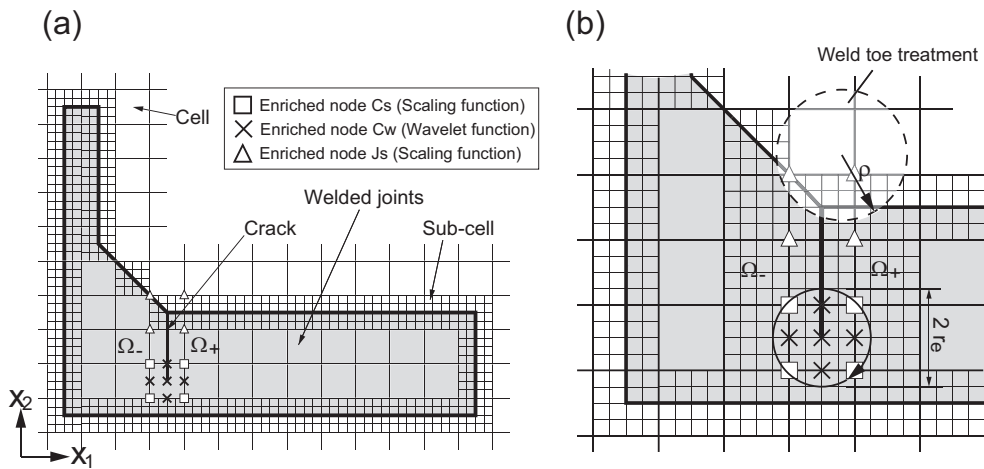


Figure 5: WX-FEM modeling of 2D welded joints.

To solve crack problems effectively, new basis functions are introduced into the wavelet FEM according to the concept of the X-FEM (WX-FEM),

to treat the crack problems and represent the displacement discontinuity of the crack surface and the high stress concentration near the crack tip. Further details of the WX-FEM are presented in [32]. A schematic illustration of the WX-FEM for the 2D welded joint structure is shown in Fig. 5 (a). The enlarged view near the welding part is shown in Fig. 5 (b). Because the WX-FEM discretization is based on fixed grids (the so-called voxel approach) [36], and it is then quite possible to model a complex shape geometry. Furthermore, a sub-cell approach is adopted to accurately represent the boundary of the body. The radius of curvature  $\rho$  of the weld toe treatment can be easily modeled employing the proposed approach as shown in Fig. 5 (b).

#### 4.2. Crack propagation simulation of a surface crack using the 2D WX-FEM and $Mk_{(2D)}$

The crack propagation is simulated using the 2D WX-FEM and  $Mk_{(2D)}$ . A schematic illustration of the approach for a surface crack in a T-shaped welded joint is presented in Fig. 6 (a). A flowchart of the crack propagation simulation is shown in Fig. 6 (b). The procedures are follows.

- (i) A 3D welded joint with a surface crack is modeled as a 2D plane strain edge cracked plate that has the same profile as the 3D welded joint. The SIF  $K$  of the edge crack is evaluated employing the 2D WX-FEM.
- (ii)  $K$  of the 2D single edge cracked plate is evaluated using the established formulae; *e.g.*, [54].
- (iii)  $Mk_{(2D)}$  is evaluated using  $K$  obtained in procedures (i) and (ii); *i.e.*,  $Mk_{(2D)} = K_{(2D \text{ welded joint})} / K_{(2D \text{ cracked plate})}$ .
- (iv)  $K$  of the surface crack in the 3D welded joint is estimated as the product of the Raju-Newman solution and  $Mk_{(2D)}$  obtained from procedure (iii).
- (v) The range of SIF  $\Delta K$  is obtained using  $K$  evaluated in procedure (iv), and the crack extends for the next step of the calculation.

Procedures (i)-(v) are repeated until the edge crack reaches the specified length. In this approach, the propagation of a surface crack in a welded joint can be simulated effectively without applying the direct 3D approach.

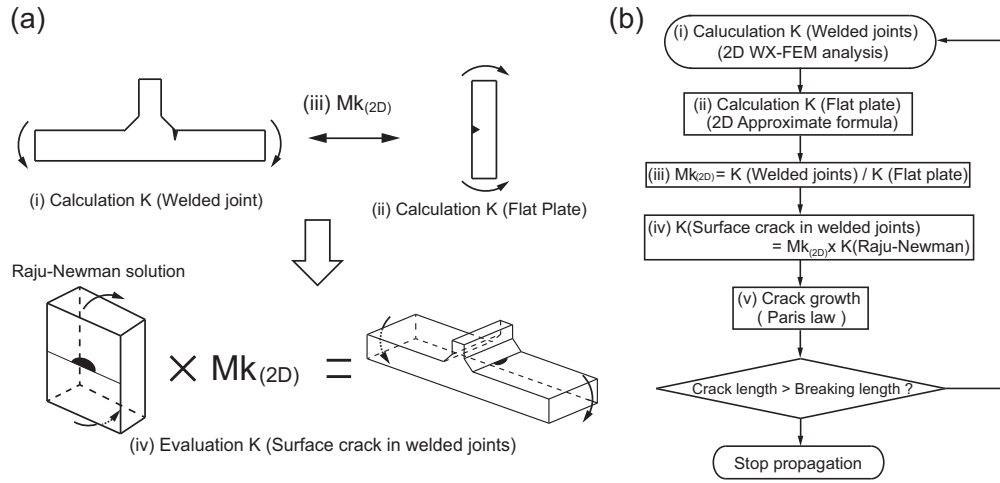


Figure 6: Crack propagation simulation using the WX-FEM and  $Mk_{(2D)}$ .

## 5. Numerical Examples

Crack propagation is simulated for surface cracks in T-shaped welded joints employing the approaches described in Chapters 2, 3 and 4. Two types of welded joints are adopted. The welded joints used in section 5.1 and 5.2 are referred to as Models A and B, respectively. The parameters are defined in Table 1.

Table 1: Parameters needed for the welded joint models.

$S$	Main plate length	$\rho$	Weld toe radius
$W$	Main plate width	$t_1$	Main plate thickness
$H$	Height of rib	$t_2$	Thickness of rib
$L$	Footprint width of rib	$l_1$	Vertical leg of welding
$\theta$	Weld angle	$l_2$	Horizontal leg of welding

The initial crack is a semi-circular surface crack at the weld toe.  $a$  is crack depth and  $c$  is crack half width. The size of the initial crack is  $a_0 = c_0 = 0.2$  mm ( $a_0/c_0 = 1.0$ ). The crack develops under cyclic loading until the crack depth reaches one-half the thickness of the main plate. The number of cycles in the final step is assumed as the fatigue crack growth life. Tensile and bending loadings are applied and the stress ratio is set to zero. A small

scale yielding condition is assumed and the welding residual stress is not considered. The material is TMCP (thermo-mechanical control process) steel and the coefficients for the Paris law are  $C = 7.24\text{e-}13$  and  $m = 3.565$  (SIF unit: MPa m<sup>1/2</sup>).

The 3D FEA using quadratic tetrahedral FEs, the 2D WX-FEM and the  $Mk_{(3D)}$  formulae are adopted for the crack propagation simulations. The SIFs,  $Mk$  factors, crack paths and fatigue cycles are examined and compared between the three approaches. In the 3D FEA, 400 nodes are used at the crack front to evaluate the SIFs. The number of nodes is maintained after the crack propagation. In the WX-FEM, level- $j$  scaling/wavelet functions and level- $j + 1$  wavelet functions are adopted. The wavelet functions are located in the radius  $r_e = 2.0$  mm from the crack tip. To check the accuracy of the WX-FEM model, 2D FEM models are also constructed using MSC.MARC MENTAT [55]. The  $J$ -integral is used to evaluate the SIFs and mode splitting of  $K_I$  and  $K_{II}$  is performed employing the crack option of MSC.MARC.

### 5.1. Analysis of a T-shaped welded joint with a radiused toe ( $\rho/t_1=0.1$ ) (Model A)

#### 5.1.1. FE modeling and evaluation of $Mk$ factors

Model A is shown in Fig. 7 (a). One-sided welding is employed and the model has a radiused weld toe ( $\rho/t_1=0.1$ ). Close-up view of the weld toe is presented in Fig. 7 (b). The surface crack is located at  $S/2$  in the longitudinal direction of the model. When the welded attachment is removed, Model A becomes a rectangular plate including a surface crack as shown in Fig. 7 (c). The model is called Model A'. The geometries are defined by the parameters shown in Table 2. Young's modulus  $E = 210$  GPa and Poisson's ratio  $\nu = 0.3$  are assumed.

Table 2: Parameters for Model A.

$S$	124 mm	$\rho$	2.2 mm
$W$	100 mm	$t_1$	22 mm
$H$	52 mm	$t_2$	18.5 mm
$L$	27.5 mm	$l_1$	9.0 mm
$\theta$	$\pi/4$	$l_2$	8.09 mm

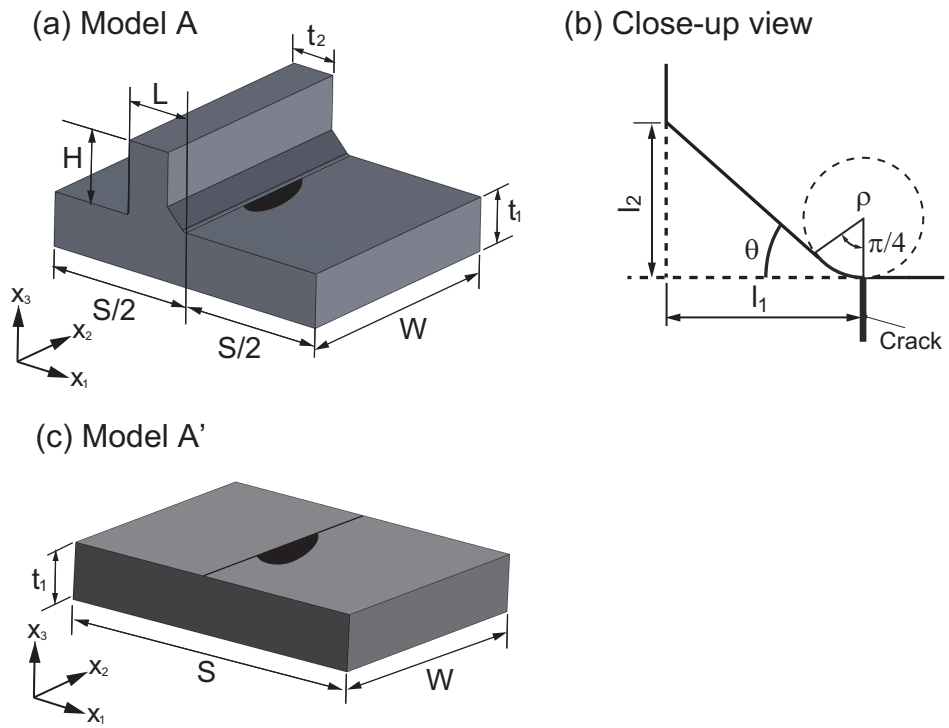


Figure 7: T-shaped welded joint (Model A).

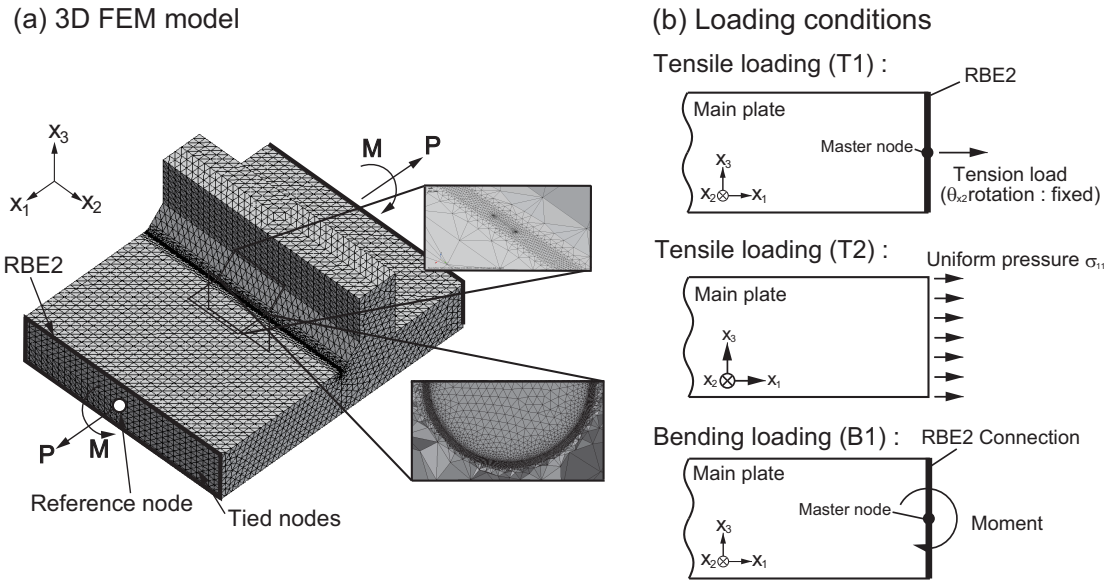


Figure 8: FE model and the boundary conditions (Model A).

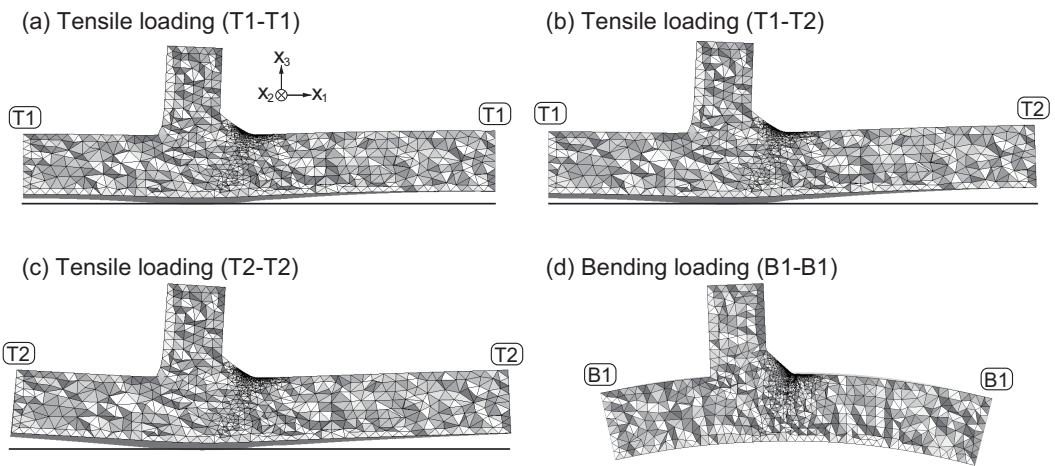


Figure 9: Deformations of Model A ( $a = c = 0.2$  mm) are visualized  $x_1 - x_3$  plane at  $x_2 = 50$  mm.

The 3D FE model including a surface crack is shown in Fig. 8 (a). The whole structure is divided into 3.0 mm tetrahedral elements and the surface crack region is divided into 0.1 mm elements. There are 0.7 million nodes and 0.45 million elements in the initial crack model. To examine  $Mk$  factors and crack propagation simulations, three kinds of boundary conditions are employed. Schematic illustrations of the loading conditions are shown in Fig. 8 (b). When tensile loading condition (T1) is chosen, force boundary conditions using Rigid Body Element 2 (RBE2) elements are adopted. RBE2 [50] is a type of rigid body element, and a tying relation can be constructed between a reference node and tied nodes. The center node of the model edge ( $x_2 - x_3$  plane) acts as the reference node and the other nodes on the  $x_2 - x_3$  plane are tied nodes as shown in Fig. 8 (a). The loads are enforced along the  $x_1$  direction, and the rotation component  $\theta_{x_2}$  is fixed on the reference nodes. When tensile loading condition (T2) is chosen, uniform pressure is employed on the edge. Therefore the rotation  $\theta_{x_2}$  of the edge is free. In addition, RBE2 is employed on the edge, and moments are enforced on the reference nodes when bending loading condition (B1) is chosen.

To check the accuracy of the FE model,  $Mk_{(3D)}$  is examined. A parametric study is performed to evaluate  $Mk_{(3D)}$  of the surface crack in Models A and A'. The surface crack dimensions  $a$  and  $c$  are varied from 0.2 to 10.0 mm ( $a/t_1=0.01-0.45$ ) while maintaining the aspect ratio  $a/c=1.0$ .  $K_I$  are evaluated at both the crack ends and the deepest point. The results are compared with the  $Mk_{(3D)}$  formulae eqs. (A5)-(A8) in [43].  $K_I$  is also calculated using Model A' to evaluate  $Mk_{(3D)}$ . The boundary condition (T1) is adopted for tensile loading case, and (B1) is adopted for bending loading case for both sides of Model A'.

The deformations of Model A ( $a = c = 0.2$  mm) with various boundary conditions are examined in Fig. 9 (a)-(c) for tensile loading case and Fig. 9 (d) for bending loading case. The deformations are visualized  $x_1 - x_3$  plane at  $x_2 = 50$  mm. When a rotation fixed boundary condition is employed both sides (T1-T1) in Fig. 9 (a), the displacement of the edges in their perpendicular directions is uniform. On the other hand, a rotation-free boundary condition is employed both sides of the model (T2-T2) in Fig. 9 (c), the edges are rotated and the local bending due to the asymmetric attachment occur near the weld toe. The local bending can also be seen when rotation free and fixed boundary conditions (T1-T2) are adopted as shown in Fig. 9

(b). Additionally, the welded joint model is deformed under bending moment as shown in Fig. 9 (d) when bending loading condition (B1-B1) is adopted.

The change in  $Mk_{(3D)}$  for  $a/t_1$  with the boundary conditions (T1-T1), (T1-T2) and (T2-T2) are examined. The  $Mk_{(3D)}$  of the crack ends and the deepest point is presented in Fig. 10 (a) and the close-up view  $a/t_1 < 0.2$  is presented in Fig. 10 (b).  $Mk_{(3D)}$  of the crack ends are larger than that of the deepest point because the high stress concentration is generated at the weld toe. Additionally, the  $Mk_{(3D)}$  are decrease as the  $a/t_1$  is larger. The  $Mk_{(3D)}$  of the analysis with the boundary condition (T1-T1) is larger than the  $Mk_{(3D)}$  with the boundary conditions (T1-T2) and (T2-T2). It is found that the local bending near the weld toe reduce the  $Mk_{(3D)}$ . The boundary conditions (T1-T1) and (B1-B1) are employed for the crack propagation simulations.

The  $Mk_{(3D)}$  is compared with the reference solutions. The results are presented in Fig.11 (a) and (b) for the tensile (T1-T1) and bending (B1-B1) loading cases. In the tensile loading case,  $Mk_{(3D)}$  approaches unity as  $a/t_1$  is increases. In contrast,  $Mk_{(3D)}$  decreases below unity when  $a/t_1$  is greater than 0.1 for the bending loading case since the welded attachment restrains the upward and opening deformations of the surface crack. The  $Mk_{(3D)}$  formulae are also presented in the figures as reference solutions. In the tensile loading case, the  $Mk_{(3D)}$  at the deepest point evaluated by the 3D FEA is good agreement with the reference solution. On the other hand, the  $Mk_{(3D)}$  at the crack ends is smaller than the formula. In the bending loading case, both the  $Mk_{(3D)}$  at the deepest point and crack ends are good agreement with the formulae. Although the trends in the values at the crack ends agree between the formula and the  $Mk_{(3D)}$ , one can find some differences in their values. It should be pointed out that when the stress intensity factor is computed using the energetic methods such as  $J$ -integral, VCCM, etc., the evaluated stress intensity factors have steep variations at the vicinity of the surface point as presented by Li *et al.* [56] and Okada *et al.* [57]. The values of the stress intensity factor at the crack ends strongly depend on the methodology, finite element mesh discretization, finite element type, etc. Therefore, the differences in the evaluated values are inevitable. Thus, it can be considered that although there are some differences between the  $Mk_{(3D)}$  and the formula at the crack ends in the tensile loading case, the change in SIF due to the stress concentration at the weld toe can be evaluated through tetrahedral FE modeling and SIF evaluations.

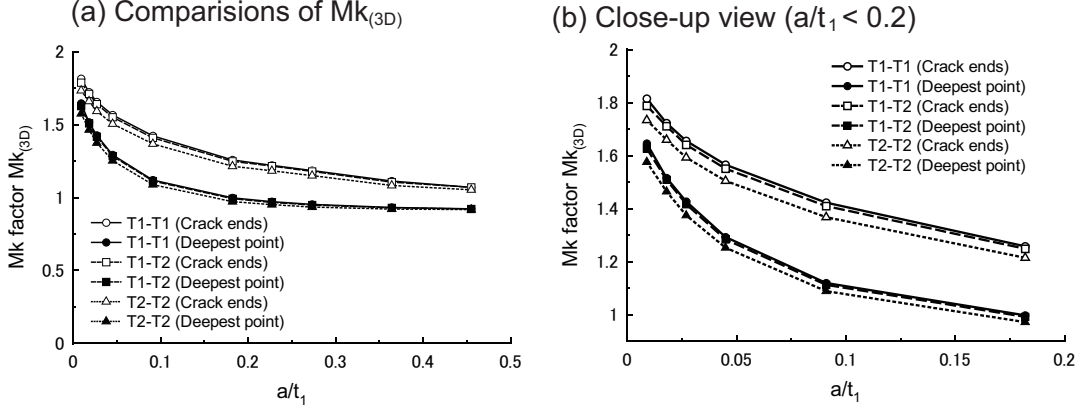


Figure 10: Comparisons of  $Mk_{(3D)}$  employing analyses with the boundary conditions T1 and T2 (Model A).

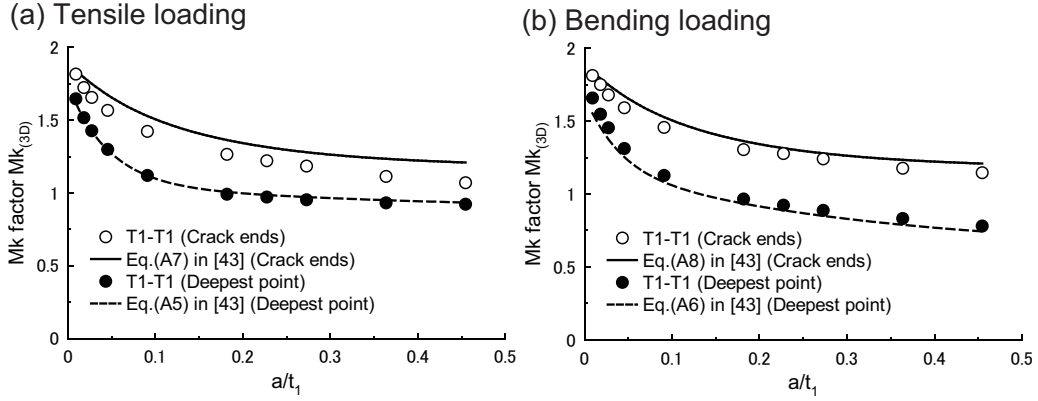


Figure 11: Comparisons of  $Mk_{(3D)}$  with the reference solutions (Model A).

The 2D WX-FEM model with an edge crack is shown in Fig. 12 (a). The whole structure is divided into equally spaced structured cells with dimensions of 0.5 mm, and the sub-cell approach is adopted to accurately represent the fillet shape and the radius of curvature at the weld toe. The length of a sub-cell is about 0.03 mm. The 2D FE model is shown in Fig. 12 (b). The whole structure is divided into 0.5 mm FEs, and very small 0.02 mm FEs

are adopted near the edge crack to evaluate the SIFs. For the tensile loading case, uniform stress  $\sigma_{11}$  is adopted at the model edges. In the bending loading case, bending moment  $M$  is enforced on the edges.

$K_I$  and  $Mk_{(2D)}$  of the WX-FEM model are compared with the reference solutions. In the tensile loading case, uniform stress  $\sigma_{11}=1.0$  (MPa) is adopted. The bending moment is adopted such that the bending stress is  $\sigma_b(= 6M/W^2)=1.0$  MPa in the bending loading case. The variations in  $K_I$  for the crack length  $a$  are shown in Fig. 13 (a).  $K_I$  of a single edge cracked plate [54] are also presented. The results of the WX-FEM are in good agreement with those of the 2D FEM. Additionally,  $K_I$  approaches the single edge cracked plate values as the crack length increases. Furthermore, the  $Mk_{(2D)}$  variations of the WX-FEM are shown in Fig. 13 (b). The results are compared with the  $Mk_{(2D)}$  formulae in [40]. High  $Mk_{(2D)}$  is obtained when  $a/t_1$  is small, and  $Mk_{(2D)}$  approaches unity as  $a/t_1$  increases. Although the formulae provide results that are larger than the WX-FEM solutions when  $a/t_1$  is small owing to the assumption of a sharp notch, they are in good agreement with each other. The comparisons confirmed that the WX-FEM can represent the high stress concentration near the weld toe with high accuracy.

### 5.1.2. Crack propagation simulation

The crack propagation simulations are carried out employing the 3D FEA, the WX-FEM and the  $Mk_{(3D)}$  formulae. Tensile and bending loadings are enforced such that the maximum tensile stress is 200 MPa and the maximum bending stress is 200 MPa. The surface crack develops every 9,000 cycles (tensile loading case) and 14,000 cycles (bending loading case) per increment. The crack paths are shown in Fig. 14 (a) and (b) for tensile and bending loading cases, respectively. In addition,  $K_I$  of the crack ends and the deepest point are presented in Fig. 15 (a) and (b), respectively. In the tensile loading case, there are small differences in  $K_I$  between the crack ends and the deepest point. The surface crack develops a semi-circular shape. In the bending loading case, the  $K_I$  of the crack ends uniformly increase but the deepest point remains constant. The surface crack thus develops a semi-elliptical shape. Furthermore, the WX-FEM well predicts  $K_I$  at the crack ends although the same  $Mk_{(2D)}$  is adopted for evaluating  $K_I$  at the deepest point and the crack ends. This is because the stress concentration at the weld toe is not so severe and there are small differences in the  $Mk$  factors between

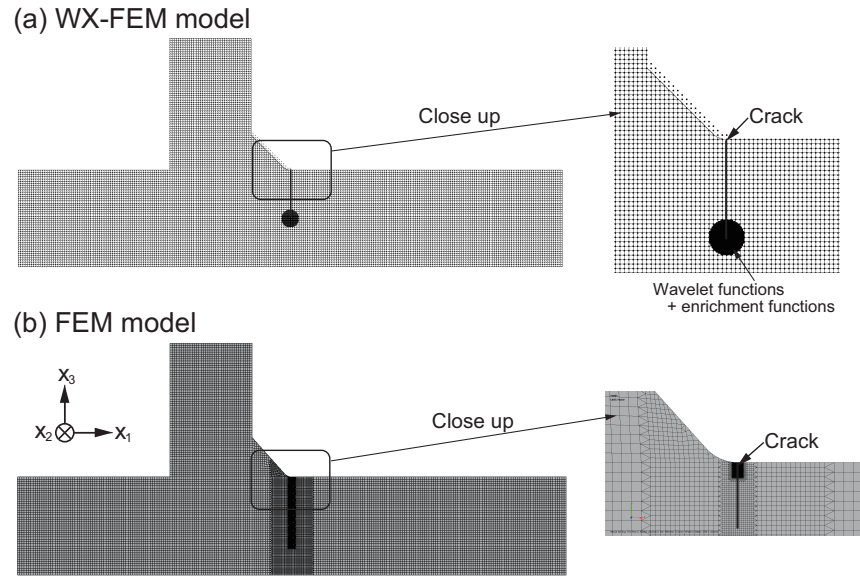


Figure 12: WX-FEM model and FEM model (Model A).

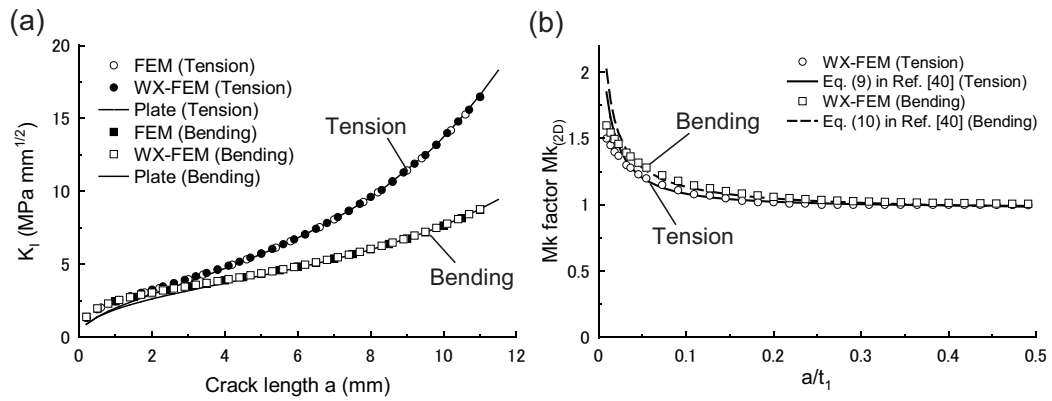


Figure 13: Comparisons of  $K_I$  and  $Mk_{(2D)}$  for tensile and bending loading cases (Model A).

the deepest point and the crack ends. It is noted that  $K_I$  evaluated by the 3D FEA is smaller than the results of the  $Mk_{(3D)}$  formulae. The differences arise from the distinction of the  $Mk_{(3D)}$  values presented in Fig. 11 (a).

The relations between the number of cycles and the crack length  $a$  are presented in Fig. 16 (a) and (b) for tensile and bending loading cases, respectively. Because the fatigue crack growth life is determined by the depth  $a$ , the fatigue life depends on  $K_I$  at the deepest point. The fatigue lives determined by 3D FEA, the WX-FEM and the  $Mk_{(3D)}$  formulae are around  $12.1 \times 10^5$ ,  $15.5 \times 10^5$  and  $8.9 \times 10^5$  cycles, respectively, for the tensile loading case, and  $17.7 \times 10^5$ ,  $17.9 \times 10^5$ , and  $14.6 \times 10^5$  cycles, respectively, for the bending loading case.  $K_I$  at the deepest points are presented in Fig. 17 (a) and (b) for  $a < 2.5$  mm. It is found that the fatigue life corresponds to the magnitude of  $K_I$  when the depth is small. Although the crack propagation simulation techniques are different, the determined fatigue lives for Model A are in good agreement.

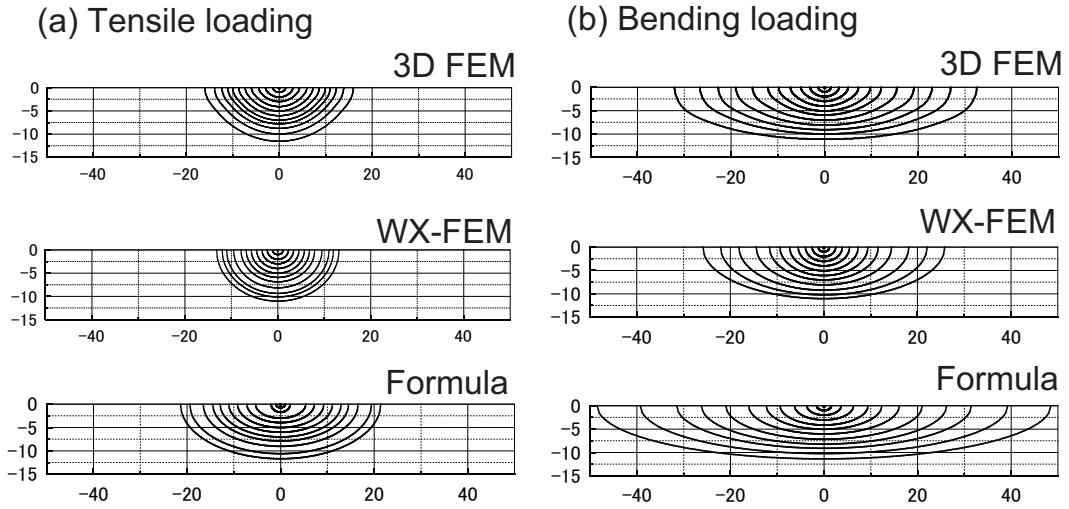
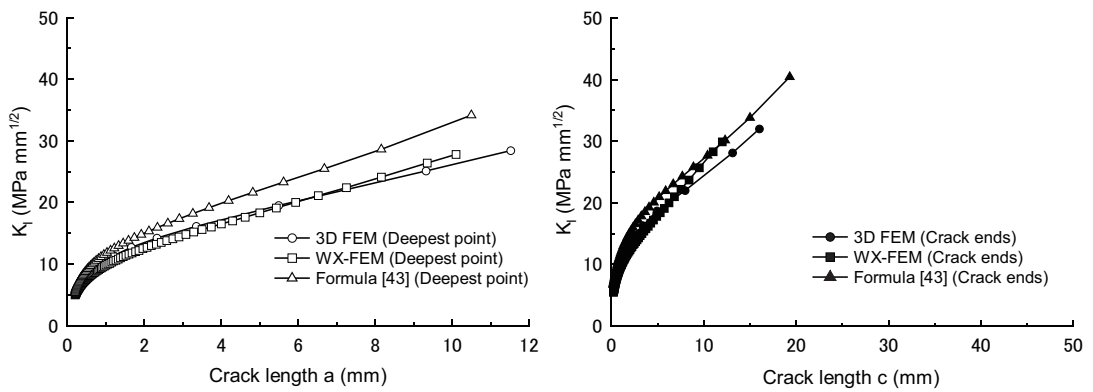


Figure 14: Crack paths in the crack propagation simulations (Model A).

(a) Tensile loading



(b) Bending loading

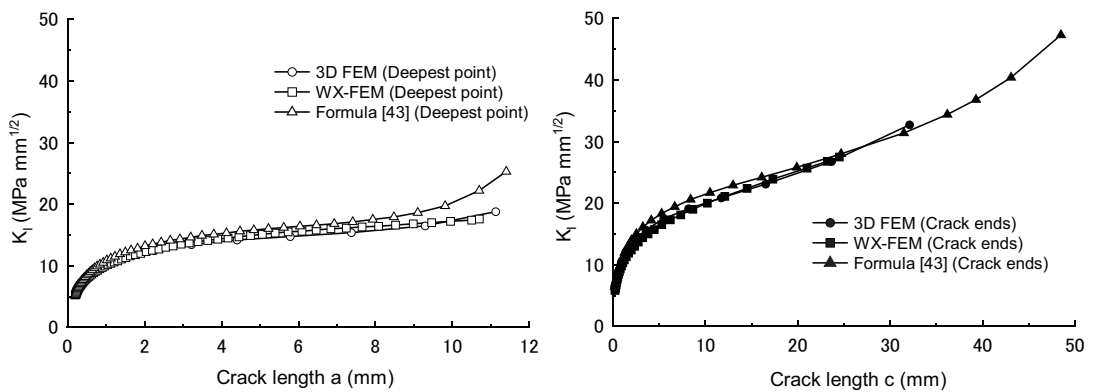
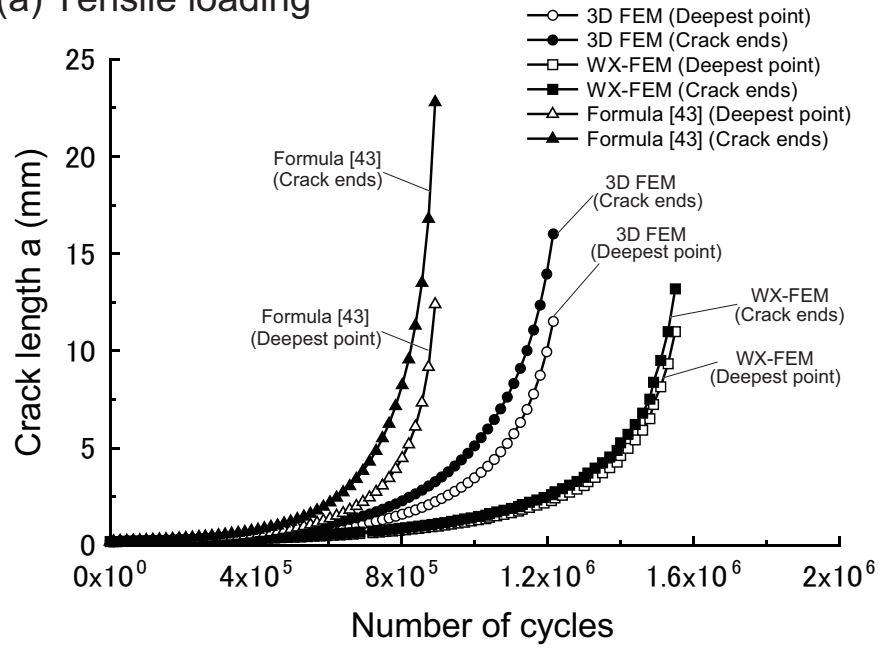


Figure 15:  $K_I$  in the crack propagation simulations (Model A).

(a) Tensile loading



(b) Bending loading

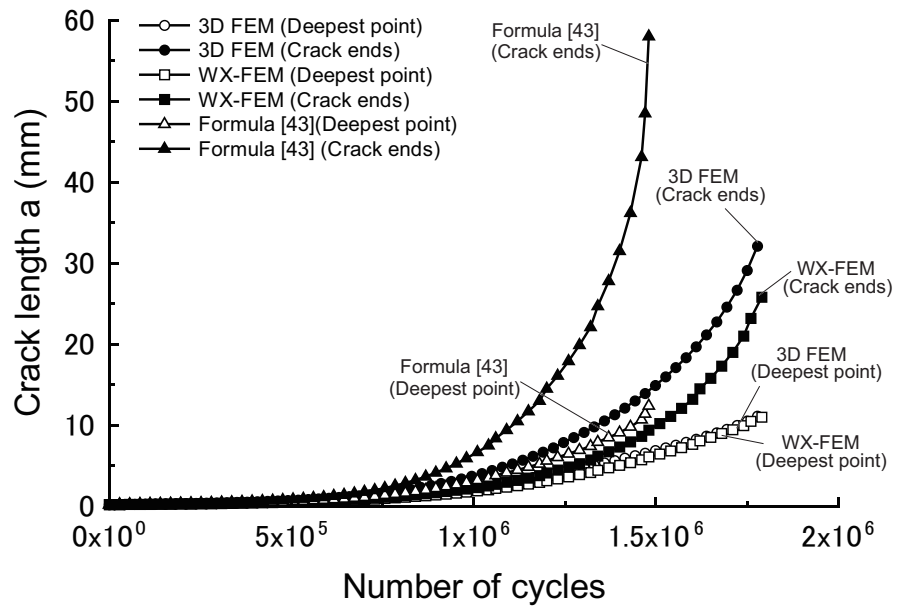


Figure 16: Relations between crack length and number of cycles (Model A).

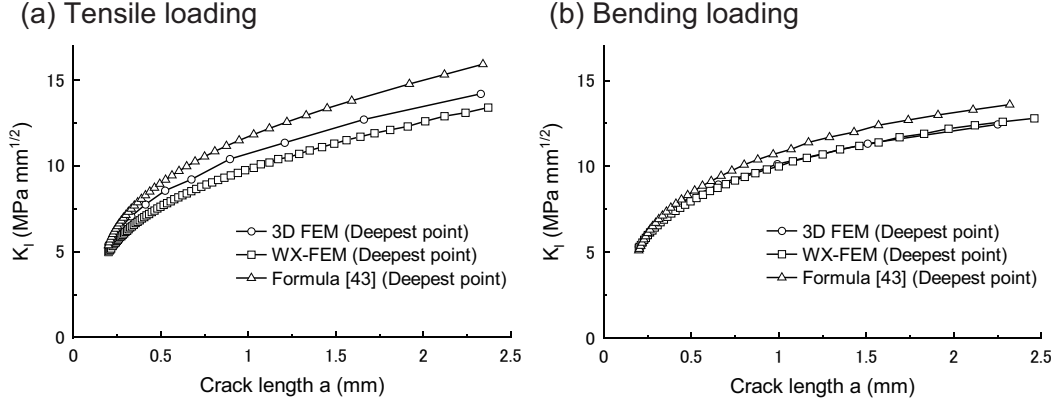


Figure 17:  $K_I$  in the crack propagation simulations ( $a < 2.5$  mm) (Model A).

## 5.2. Analysis of the T-shaped welded joint with a ground weld toe (Model B)

### 5.2.1. FE modeling and evaluation of $Mk$ factors

Crack propagation simulations for Model B are carried out. Model B is presented in Fig. 18 (a). The model has a ground weld toe. Young's modulus is  $E = 206$  GPa and Poisson's ratio is  $\nu = 0.3$ . The main plate is ground 0.4 mm from the surface to remove the undercut. The parameters are set as shown in Fig. 18 (b). The model was used in the SR202 report (Shipbuilding research committee 202) [58] and the fatigue strength evaluation was discussed employing fatigue tests and numerical simulations. The initial crack is located at the deepest point of the radiused toe. To the authors' knowledge, there is no  $Mk_{(3D)}$  formulae for the ground weld toe. The results are therefore compared with those obtained with 3D FEA and the 2D WX-FEM. The SR202 numerical results are also adopted as reference solutions although there was no detailed discussion of the accuracy in that report.

The 3D FEA model with a surface crack is shown in Fig. 19. A half model is adopted because of the symmetry property of the problem. There are 0.45 million nodes and 0.3 million elements in the initial crack model. A bending loading is enforced. The bending moment and symmetrical boundary condition are enforced on the 3D FEA model as shown in Fig. 19. The WX-FEM model with an edge crack is presented in Fig. 20 (a). A half model is again adopted. To check the accuracy of the WX-FEM model, the 2D FEM model is arranged as shown in Fig. 20 (b). The boundary condi-

tions of the WX-FEM and FEM models are shown in Fig. 20 (a) and (b). The mesh divisions of the 3D FEA, WX-FEM model and 2D FEM model are the same as those of Models A and B.

The results of  $K_I$  are presented in Fig. 21 (a) for the WX-FEM, the 2D FEM, the SR202 report and a single edge cracked plate. In the SR202 report,  $K_I$  was evaluated using a finite element substructure model [59]. The crack length  $a'$  ( $a' = a + 0.4$  mm) is defined as shown in Fig. 21 (b). Although there are differences between the results of the WX-FEM and the SR202 report, the WX-FEM results correspond to the 2D FEM results. In addition,  $K_I$  of the WX-FEM approaches that of a single edge cracked plate as the crack length is increases. It is thus confirmed that the WX-FEM results provide highly accurate solutions for Model B.

In addition,  $Mk_{(2D)}$  is examined. Because the weld toe is ground, two kinds of crack lengths  $a$  and  $a'$  can be considered when evaluating  $K_I$  for a single edge cracked plate. The  $K_I$  values and the  $Mk_{(2D)}$  for the WX-FEM model and the single edge cracked plate are shown in Table 4. When the crack length  $a'$  is chosen, very small  $Mk_{(2D)}$  is obtained. The crack length  $a$  is then adopted in evaluating  $Mk_{(2D)}$  although  $Mk_{(2D)}$  is slightly larger than unity as the crack length increases.

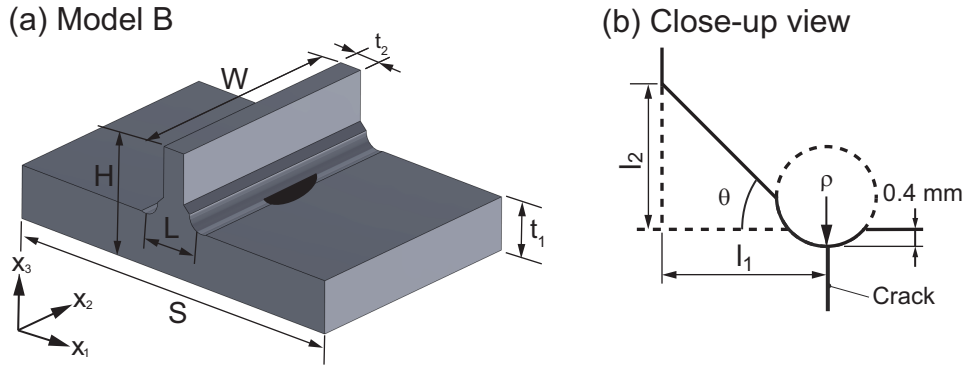


Figure 18: T-shaped welded joint (Model B).

Table 3: Parameters for Model B.

$S$	152 mm	$\rho$	6.0 mm
$W$	100 mm	$t_1$	22 mm
$H$	52 mm	$t_2$	10.0 mm
$L$	28 mm	$l_1$	9.0 mm
$\theta$	$\pi/4$	$l_2$	9.0 mm

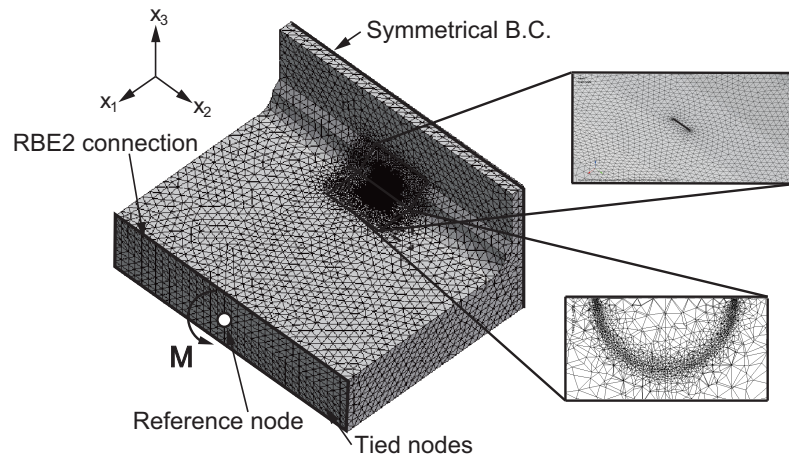


Figure 19: FE model and boundary conditions (Model B).

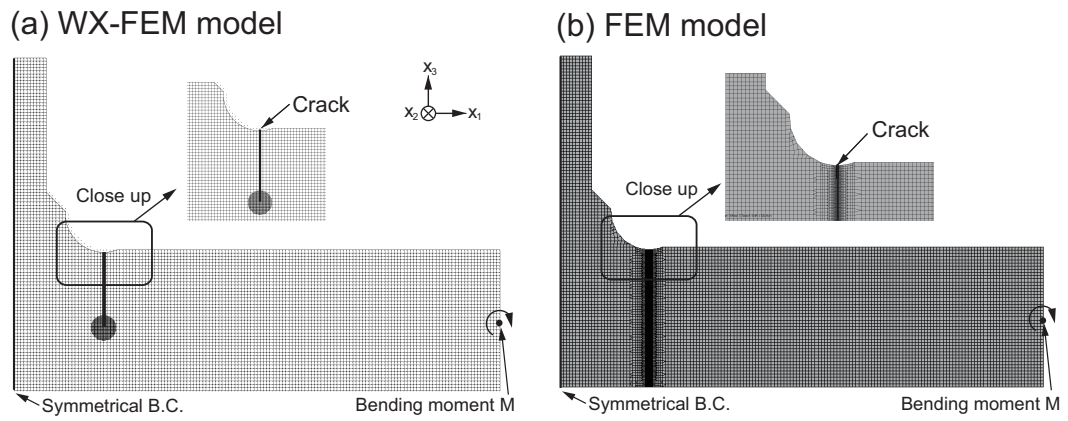


Figure 20: WX-FEM model and FEM model (Model B).

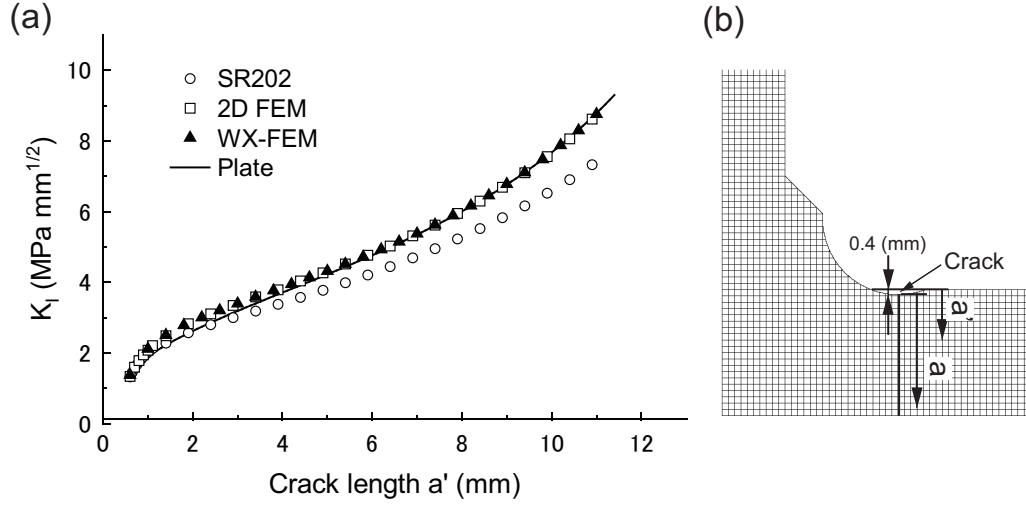


Figure 21: Comparisons of  $K_I$  and  $Mk_{(2D)}$  (Model B).

Table 4: Variations of  $K_I$  and  $Mk_{(2D)}$  of Model B ( $K_I$  unit:  $\text{MPa mm}^{1/2}$ ).

$a$ ( $a'$ )	$K_I^{WX-FEM}$	$K_I^{Plate}(a)$	$Mk_{(2D)}(a)$	$K_I^{Plate}(a')$	$Mk_{(2D)}(a')$
0.2 (0.6)	1.38	0.88	1.57	1.50	0.92
1.0 (1.4)	2.51	1.90	1.32	2.22	1.13
3.0 (3.4)	3.59	3.19	1.12	3.40	1.05
5.0 (5.4)	4.52	4.23	1.07	4.44	1.02
7.0 (7.4)	5.63	5.35	1.05	5.60	1.00
9.0 (9.4)	7.11	6.77	1.05	7.11	1.00
11.0 (11.4)	9.26	8.79	1.05	9.30	1.00

### 5.2.2. Crack propagation simulation

The crack propagation is simulated for Model B. The results of the 3D FEA, 2D WX-FEM and the SR202 report are compared. Four bending loadings are adopted to provide maximum bending stresses of 130, 150, 200 and 300 MPa, and the surface crack develops every  $6.0 \times 10^4$ ,  $4.0 \times 10^4$ ,  $1.5 \times 10^4$  and  $0.3 \times 10^4$  cycles, respectively.

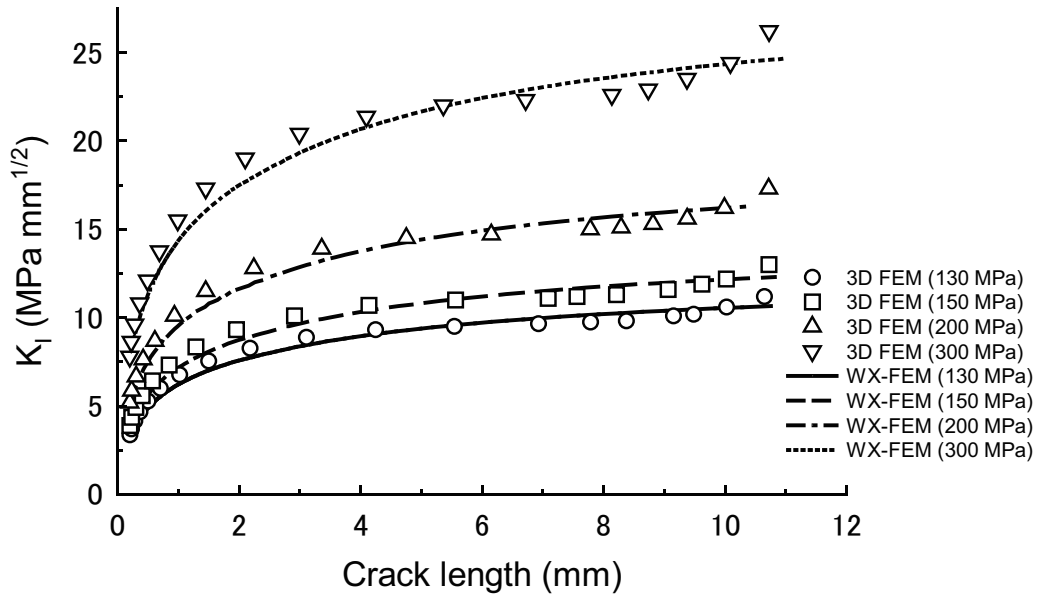


Figure 22:  $K_I$  for the crack propagation simulations (Model B).

$K_I$  values at the deepest point are shown in Fig. 22 for the 3D FEA and WX-FEM. The results of 3D FEA are in good agreement with those of the WX-FEM for all crack lengths. The relation between the number of cycles and crack length  $a$  is shown in Fig. 23. The results are in good agreement in all loading cases. Additionally, the fatigue lives of the 3D FEAs and the WX-FEM are summarized in Table 5. The results of the SR202 report are digitized from the report. Although the approaches of the crack propagation simulations are different, the results show good correlation. It is thus confirmed that the approach used in this study can be adopted to determine the fatigue crack growth life of a surface crack in a welded joint.

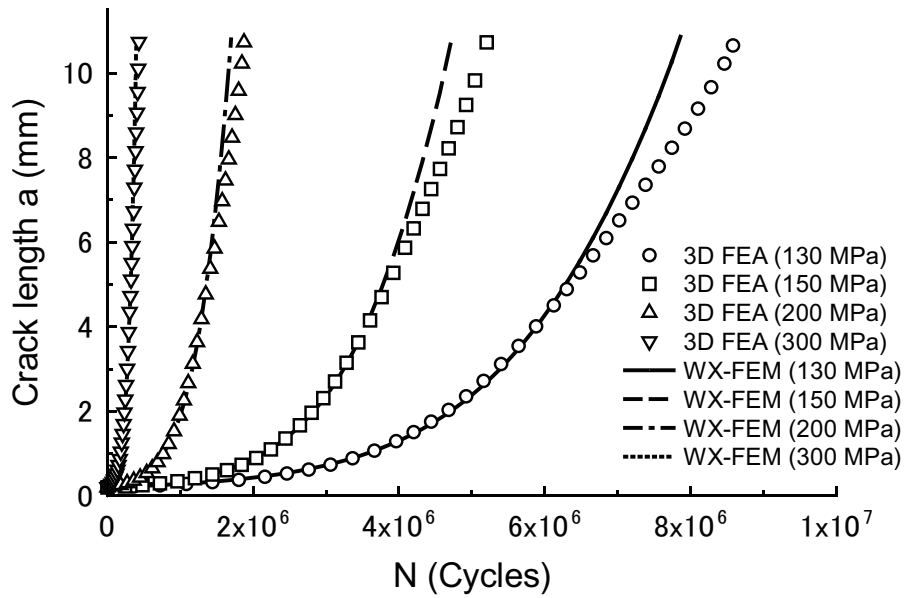


Figure 23: Relations between crack length and number of cycles (Model B).

Table 5: Fatigue crack growth lives (Model B).

	3D-FEA	WX-FEM	SR202
130 MPa	$8.58 \times 10^6$	$7.86 \times 10^6$	$6.30 \times 10^6$
150 MPa	$5.20 \times 10^6$	$4.72 \times 10^6$	$3.87 \times 10^6$
200 MPa	$1.88 \times 10^6$	$1.70 \times 10^6$	$1.38 \times 10^6$
300 MPa	$4.32 \times 10^6$	$3.96 \times 10^6$	$3.34 \times 10^6$

In the numerical examples, crack propagation simulations were performed using the 3D FEA, the WX-FEM and  $Mk_{(3D)}$  formulae for a surface crack in a T-shaped welded joint. When using the  $Mk_{(3D)}$  formulae, the crack propagation was easily simulated with simplified formulae and the calculation required a very short computational time. Employing the WX-FEM, 2D propagation of an edge crack could be simulated with high accuracy without remeshing procedures and a highly accurate  $Mk_{(2D)}$  was obtained. In addition, propagation of a surface crack in a welded joint was simulated using the  $Mk_{(2D)}$  and Raju-Newman solution. In the 3D FEA using quadratic tetrahedral FEs, although large-scale computation was needed, highly accurate SIFs were obtained and there was no need to assume a semi-circular shape of the surface crack. It will thus be possible to simulate propagation of a surface crack located in an arbitrary position of a welded joint. Although the above techniques are different, the results obtained for  $K_I$ , crack lengths and crack paths are in good agreement. It is thus confirmed that the approaches used in this study can be used to simulate crack propagation and predict the fatigue crack growth life for a surface crack in a welded joint.

## 6. Conclusion

In this paper, propagation of surface cracks in T-shaped welded joints was simulated using new approaches of computational fracture mechanics. Two computational approaches were adopted. One was the 3D FEA using quadratic tetrahedral FEs and the other was the 2D WX-FEM and the  $Mk_{(2D)}$ . The results were compared with results obtained with  $Mk_{(2D)}$  and  $Mk_{(3D)}$  formulae. The SIFs,  $Mk$  factors, crack paths and fatigue cycles were compared. The accuracy and effectiveness of the proposed approaches were discussed with the numerical examples. It was confirmed that the approaches of computational fracture mechanics and the crack propagation simulations were effective in evaluating the fatigue strength of welded joints.

## Acknowledgements

I would like to thank Y. Kobayashi and S. Masahiro (TechnoStar Co., Ltd.) for supporting crack propagation simulation using 3D FEA. This work was performed under the Cooperative Research Program of Institute for Joining and Welding Research Institute, Osaka University.

## References

- [1] Suresh S. Fatigue of materials, 2nd *ed.*. Cambridge University Press, 2002.
- [2] Anderson TL. Fracture mechanics: Fundamentals and applications 3rd *ed.*. CRC Press, 2005.
- [3] Maddox SJ. Fatigue strength of welded structures, 2nd *ed.*. Woodhead Publishing, 2002.
- [4] Ritchie RO. Mechanisms of fatigue-crack propagation in ductile and brittle solids. *Int J Fract* 1999;100:55-83.
- [5] Fricke W. Fatigue analysis of welded joints: state of development. *Mar Struct* 2003;16:185-200.
- [6] Maddox SJ. An analysis of fatigue cracks in fillet welded joints. *Int J Fract* 1975;11:221-43.
- [7] Newman Jr JC, Raju IS. An empirical stress-intensity factor equation for the surface crack. *Eng Fract Mech* 1981;15:185-92.
- [8] Paris P, Erdogan F. A critical analysis of crack propagation laws. *Trans ASME J Basic Eng* 1963;85:528-34.
- [9] BS7910. Guide to methods for assessing the acceptability of flaws in metallic structures. British Standards Institution, 2007.
- [10] WES2805. Method of assessment for flaws in fusion welded joints with respect to brittle fracture and fatigue crack growth. The Japan Welding Engineering Society, 2007.
- [11] Kam JCP, Dover WD, Ma CN. The prediction of crack shape development for in-service cracks in offshore welded tubular joints. *Mar Struct* 1995;8:37-65.
- [12] Sumi Y. Fatigue crack propagation and computational remaining life assessment of ship structures. *J Mar Sci Tech* 1998;3:102-12.
- [13] Mahmoud HN, Dexter RJ. Propagation rate of large cracks in stiffened panels under tension loading. *Mar Struct* 2005;18:265-88.

- [14] Okawa T, Sumi Y, Mohri M. Simulation-based fatigue crack management of ship structural details applied to longitudinal and transverse connections. *Mar Struct* 2006;19:217-40.
- [15] Seifi R, Omidvar N. Fatigue crack growth under mixed mode I + III loading. *Mar Struct* 2013;34:1-15.
- [16] He W, Liu J, Xie D. Numerical study on fatigue crack growth at a web-stiffener of ship structural details by an objected-oriented approach in conjunction with ABAQUS. *Mar Struct* 2014;35:45-69.
- [17] Nishioka T, Tokudome H, Kinoshita M. Dynamic fracture-path prediction in impact fracture phenomena using moving finite element method based on Delaunay automatic mesh generation. *Int J Solid Struct* 2001;38:5273-301.
- [18] Rajaram H, Socrate S, Parks DM. Application of domain integral methods using tetrahedral elements to the determination of stress intensity factors. *Eng Fract Mech* 2000;66:455-82.
- [19] Nagai M, Ikeda T, Miyazaki N. Stress intensity factor analyses of three-dimensional interface cracks using tetrahedral finite elements. *Comput Mech* 2013;51:603-15.
- [20] Okada H, Kawai H, Tokuda T, Fukui Y. Fully automated mixed mode crack propagation analyses based on tetrahedral finite element and VCCM (Virtual crack closure-integral method). *Int J Fatig* 2013;50:33-9.
- [21] Belytschko T, Lu YY, Gu L. Element-free Galerkin methods. *Int J Numer Meth Eng* 1994;37:229-56.
- [22] Fleming M, Chu YA, Moran B, Belytschko T. Enriched element-free Galerkin methods for crack tip fields. *Int J Numer Meth Eng* 1997;40:1483-504.
- [23] Belytschko T, Black T. Elastic crack growth in finite elements with minimal remeshing. *Int J Numer Meth Eng* 1999;45:601-20.
- [24] Moës N, Dolbow J, Belytschko T. A finite element method for crack growth without remeshing. *Int J Numer Meth Eng* 1999;46:131-50.

- [25] Yagawa G, Yamada T. Free mesh method: A new meshless finite element method. *Comput Mech* 1996;18:383-6.
- [26] Yagawa G, Furukawa T. Recent developments of free mesh method. *Int J Numer Meth Eng* 2000;47:1419-43.
- [27] Cisilino AP, Aliabadi MH. Three-dimensional boundary element analysis of fatigue crack growth in linear and non-linear fracture problems. *Eng Fract Mech* 1999;63:713-33.
- [28] Cisilino AP, Aliabadi MH. Three-dimensional BEM analysis for fatigue crack growth in welded components. *Int J Pres Ves Pip* 1997;70:135-44.
- [29] Chen T, Xiao ZG, Zhao XL, Gu XL. A boundary element analysis of fatigue crack growth for welded connections under bending. *Eng Fract Mech* 2013;98:44-51.
- [30] <http://en.e-technostar.com/> [Accessed date:15 July 2014]
- [31] Okada H, Kawai H, Araki K. A virtual crack closure-integral method (VCCM) to compute the energy release rates and stress intensity factors based on tetrahedral finite elements. *Eng Fract Mech* 2008;75:4466-85.
- [32] Tanaka S, Okada H, Okazawa S, Fujikubo M. Two-dimensional fracture mechanics analyses using the wavelet Galerkin method and extended finite element method. *Int J Numer Meth Eng* 2013;93:1082-108.
- [33] Amaratunga K, Williams JR, Qian S, Weiss J. Wavelet-Galerkin solutions for one dimensional partial differential equations. *Int J Numer Meth Eng* 1994;37:2703-16.
- [34] Diaz AR. A wavelet-Galerkin scheme for analysis of large-scale problems on simple domains. *Int J Numer Meth Eng* 1999;44:1599-616.
- [35] Tanaka S, Okada H, Okazawa S. A wavelet Galerkin method employing B-spline bases for solid mechanics problems without the use of a fictitious domain. *Comput Mech* 2012;50:35-48.
- [36] Hollister SJ, Kikuchi N. Homogenization theory and digital imaging: A basis for studying the mechanics and design principles of bone tissue. *Biotechnol Bioeng* 1994;43:586-96.

- [37] Niu X, Glinka G. The weld profile effect on stress intensity factors in weldments. *Int J Fract* 1987;35:3-20.
- [38] Hobbacher A. Stress intensity factors of plates under tensile load with welded-on flat side gussets. *Eng Fract Mech* 1992;41:897-905.
- [39] Hobbacher A. Stress intensity factors of welded joints. *Eng Fract Mech* 1993;46:173-82.
- [40] Fu B, Haswell JV, Bettess P. Weld magnification factors for semi-elliptical surface cracks in fillet welded T-butt joint models. *Int J Fract* 1993;63:155-71.
- [41] Bowness D, Lee MMK. The development of an accurate model for the fatigue assessment of doubly curved cracks in tubular joints. *Int J Fract* 1995;73:129-47.
- [42] Bowness D, Lee MMK. Stress intensity factor solutions for semi-elliptical weld-toe cracks in T-butt geometries. *Fatig Fract Eng Mater Struct* 1996;19:787-97.
- [43] Bowness D, Lee MMK. Prediction of weld toe magnification factors for semi-elliptical cracks in T-butt joints. *Int J Fatig* 2000;22:369-87.
- [44] Bowness D, Lee MMK. Weld toe magnification factors for semi-elliptical cracks in T-butt joints - comparison with existing solutions. *Int J Fatig* 2000;22:389-96.
- [45] Lee MMK, Bowness D. Estimation of stress intensity factor solutions for weld toe cracks in offshore tubular joints. *Int J Fatig* 2002;24:861-75.
- [46] Rice JR. A path independent integral and the approximate analysis of strain concentration by notches and cracks. *J Appl Mech* 1968;35:379-86.
- [47] Hellen TK. On the method of virtual crack extensions. *Int J Numer Meth Eng* 1975;9:187-207.
- [48] Irwin GR. Fracture. in *Handbuch der Physik* 6, edited by S. Flugge. 551-90. Springer-Verlag Berlin-Heidelberg, 1958.

- [49] Rybicki EF, Kanninen MF. A finite element calculation of stress intensity factors by a modified crack closure integral. *Eng Fract Mech* 1977;9:931-8.
- [50] MD Nastran R3.1, Quick Reference Guide.
- [51] Chui CK. An introduction to wavelets. Academic Press, 1992.
- [52] Daubechies I. Ten Lectures on Wavelets. SIAM, Philadelphia, 1992.
- [53] Yau JF, Wang SS. An analysis of interface cracks between dissimilar isotropic materials using conservation integrals in elasticity. *Eng Fract Mech* 1984;20:423-32.
- [54] Murakami Y *ed.*. Stress intensity factors handbook. Pergamon Press, 1986.
- [55] MSC.Marc 2005r3, User's Guide.
- [56] Li Y, Itoh H, Hasegawa K, Oskabe K, Okada H. Development of stress intensity factors for deep surface cracks in plates and cylinders. In: 2012 ASME Pressure Vessels and Piping Division Conference, Toronto, 15th-19th July 2012; 2012. PVP 2012-78109.
- [57] Okada H, Higashi M, Kikuchi M, Fukui Y, Kumazawa N. Three dimensional virtual crack closure-integral method (VCCM) with skewed and non-symmetric mesh arrangement at the crack front. *Eng Fract Mech* 2005;72:1717-37.
- [58] SR202. Report of research on offshore structure design methodology and weld quality; 202 research committee of the shipbuilding research association of Japan, 1991. (in Japanese)
- [59] Higuchi M, Kawahara M, Kondo K. Calculation of stress intensity factors by a finite element substructure model. *Journal of the Japan Society of Naval Architects and Ocean Engineers* 1974;135:327-35. (in Japanese)